

# Mass and energy balance calculations for an artificial ice reservoir (Icestupa)

Suryanarayanan Balasubramanian<sup>1,\*</sup>, Martin Hoelzle<sup>1</sup>, Michael Lehning<sup>2</sup>,  
Sonam Wangchuk<sup>3</sup>, Johannes Oerlemans<sup>4</sup> and Felix Keller<sup>5</sup>

<sup>1</sup> University of Fribourg, Fribourg, Switzerland

<sup>2</sup> WSL Institute for Snow and Avalanche Research, Davos, Switzerland

<sup>3</sup> Himalayan Institute of Alternatives Ladakh, Leh, India

<sup>4</sup> Institute for Marine and Atmospheric Research, Utrecht University, Utrecht, The Netherlands

<sup>5</sup> Academia Engiadina, Samedan, Switzerland

Correspondence\*:

Suryanarayanan Balasubramanian

suryanarayanan.balasubramanian@unifr.ch

## 2 ABSTRACT

Artificial Ice Reservoirs (AIRs) can successfully store water during winter and release the water during spring and summer. This makes them a reliable fresh water resource for irrigation in dry environments. Several AIRs have been built but studies of their water storage capacity and efficiency are scarce. This study models a cone-shaped AIR popularly called Icestupa. Processes involved in the development and temporal evolution of an Icestupa are calculated by a physically-based model using equations governing the heat transfer, vapour diffusion and transport of water that undergoes phase changes. These processes were quantified using meteorological data in conjunction with fountain spray information (mass input of an Icestupa) to estimate the quantity of frozen, melted, evaporated and runoff water at a location called 'Eispalast' in Fribourg, Switzerland. At this measurement site, an Icestupa was built for model validation purposes. The model was further tested by performing a sensitivity and uncertainty study showing that the most sensitive parameters are the ice emissivity and the temperature threshold used to determine precipitation phase. Model calculations estimate that the Eispalast Icestupa stored about 5% of the total water sprayed as ice. In addition, we found that reducing nozzle diameter of the fountain from 5 mm to 3 mm increases the water storage up to 78% without compromising on the storage duration.

Keywords: ictestupa, mass balance, water storage, climate change adaptation, geoengineering

## 1 INTRODUCTION

Seasonal snow cover, glaciers and permafrost are expected to change their water storage capacity due to climate change with major consequences for downriver water supply (Immerzeel et al., 2019). The challenges brought about by these changes are especially important for dry mountain environments such as in Central Asia or the Andes, which directly rely on the seasonal meltwater for their farming and drinking needs (Hoelzle et al., 2019; Apel et al., 2018; Buytaert et al., 2017; Chen et al., 2016; Unger-Shayesteh



**Figure 1.** Icestupa in Ladakh, India on March 2017 was 24 m tall and contained around 3700  $m^3$  of water. Picture Credits: Lobzang Dadul

25 et al., 2013). Some villages in Ladakh, India have already been forced to relocate due to glacial retreat and  
26 the corresponding loss of their main fresh water resources (Grossman, 2015).

27 Artificial ice reservoirs (AIRs) have been considered to be a feasible way to adapt to these changes (Hock  
28 et al., 2019; Nüsser et al., 2019b). An AIR is a human-made ice structure typically constructed during the  
29 cold winter months and designed to slowly release freshwater during the warm and dry spring and summer  
30 months. The main purpose of AIRs is irrigation. Therefore, AIRs are designed to store water in the form of  
31 ice as long into the summer as possible. The energy required to construct an AIR is usually derived from  
32 the gravitational head of the source water body. Some are constructed horizontally by freezing water using  
33 a series of checkdams and others are built vertically by spraying water through fountain systems (Nüsser  
34 et al., 2019a). The latter are colloquially referred to as Icestupas and are the subject of this study.

35 A typical Icestupa just requires a pipeline attached to a vertically mounted metal pipe with a fountain  
36 nozzle for construction. Their water source is usually a high altitude lake or glacial stream. Due to the  
37 altitude difference between the pipeline input and fountain output, water ejects from the fountain nozzle as  
38 droplets that eventually lose their latent heat to the atmosphere and accumulate as ice around the metal pipe.  
39 The fountain nozzle is raised through addition of further pipes as and when significant ice accumulates.  
40 Typically, a dome of branches is constructed around the metal pipe so that such pipe extensions can be  
41 done from within this dome. During the winter, the fountain is manually activated from sunset to sunrise.  
42 Threads, tree branches and fishing nets are used to guide and accelerate the ice formation.

43 Since their invention in 2013 (Wangchuk, 2014), Icestupas have gained widespread publicity in the region  
44 of Ladakh, Northern India since they require very little infrastructure, skills and energy to be constructed  
45 in comparison to other water storage technologies. Compared to other AIR geometries, Icestupas (Fig.  
46 1) can be built at lower altitudes and last much longer into the summer than other types of ice structures  
47 (Wangchuk, 2014). However, to date, no reliable estimates exist about the amount of sprayed water that  
48 is necessary to create them and the meltwater they provide (Nüsser et al., 2019a). Rough estimates of  
49 Icestupa meltwater in Ladakh suggest that the water loss during the construction process is considerable  
50 (see Appendix 8.1). A complete set of measurements of the water storage and energy balance are required  
51 to understand the cause of the water losses better and increase the construction efficiency.

In this paper, we aim to develop a physically-based model of a vertical AIR (or Icestupa) that can quantify their storage efficiency using existing weather and water usage information. Mass and energy balance equations were used to estimate the quantity of water frozen, melted, evaporated and runoff. Sensitivity and uncertainty analysis were performed to identify the most critical parameters and the variance caused by them. For validation, we created an Icestupa at an accessible site (called Eispalast) near Schwarzsee close to the city of Fribourg, Switzerland, allowing easy maintenance and control of the measurements. Due to the low altitude of the site with relatively high winter temperatures, only a small Icestupa could be established during winter 2018/19 to provide us with model validation data. Our model and validation experiments provide first steps towards evaluating the effectiveness of a vertical AIR for irrigation and allow us to outline some preliminary guidelines for consideration when a construction of an Icestupa for water storage is envisaged.

## 2 STUDY SITE

The Eispalast (EP) site in the Schwarzsee region lies at 967 m a.s.l.. In the winter (Oct-Apr), mean daily maximum and minimum air temperatures vary between -4 and 14 °C. Clear skies are rare, averaging around 7 days, and precipitation amounts average 155 mm per month during winter (Meteoblue, 2020). The site was situated adjacent to a stream resulting in high humidity values across the study period. Within the EP site, an enclosure with a 1.8 m radius was constructed for the experiment. An automatic weather station (AWS) was adjacent to the wooden boundary as shown in Fig. 2. The fountain used for spraying water had a nozzle diameter of 5 mm and a height of 1.35 m, and was placed in the centre of the wooden enclosure. The water was transferred from a spring water source at 1267 m a.s.l. by pipeline and flowed via a flowmeter and an air escape valve to the nozzle, where it was sprinkled with a spray radius of around 1.7 m. The air escape valve was installed to avoid errors in the flow measurements due to air bubbles. In addition, a webcam guaranteed a continuous survey of the site during the construction of the Icestupa.

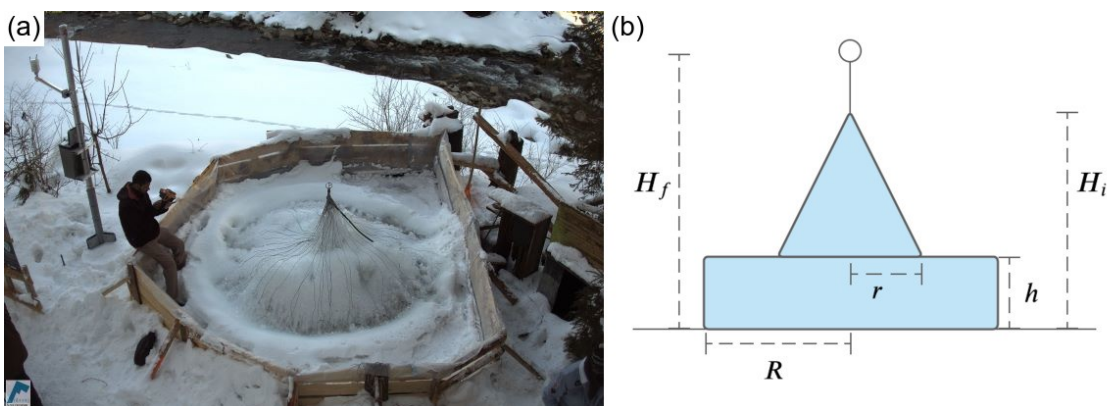


**Figure 2.** (a) The ice structure during the first validation measurement as seen on the webcam image of 14<sup>th</sup> Feb. (b) The corresponding cross section of the EP ice structure with the field estimates of  $r$ ,  $R$ ,  $h$ ,  $H_i$ ,  $H_f$  used to determine the Icestupa volume is shown on the right.

### 2.1 Construction

From 30<sup>th</sup> January to 18<sup>th</sup> March 2019 the Icestupa was constructed through the fountain spray, which was manually switched on if measured air temperature was below -5 °C after sunset and was switched off as soon as the ice was exposed to daylight or temperatures were above 0 °C. The water spray of the fountain was initially adjusted so that most of the water droplets land within the wooden boundary zone. The ice formation was guided by adding a metal framework at the ice structure base after the first night of

80 operation. Several cotton threads were tied between the ice structure base and fountain pole for accelerating  
 81 and further guiding the ice formation process.

## 82 2.2 Measurements and Data

83 Measurements comprising air temperature, relative humidity, water flow rate, wind speed and direction  
 84 were made every 5 minutes throughout the construction period. The water flow rate or discharge was  
 85 measured via an ultrasonic sensor attached to the fountain supply pipeline. Precipitation data was derived  
 86 from the Plaffeien AWS (IDAWEB, 2019) located 8.8 km away from the measurement site at an altitude of  
 87 1042 m a.s.l.

88 In addition, we used ERA5 reanalysis dataset (Copernicus Climate Change Service (C3S), 2017) for  
 89 filling data gaps and adding data that were not measured directly at the EP site. We recognised during  
 90 our data analysis that, except precipitation, all the other meteorological variables of the EP site correlated  
 91 much better with the ERA5 dataset than the nearby Plaffeien AWS dataset. The 2 m temperature parameter  
 92 correlated with air temperature ( $r^2 = 0.9$ ), surface pressure parameter correlated with air pressure ( $r^2 = 1$ )  
 93 and 10m wind speed parameter (derived from horizontal and vertical components) correlated with wind  
 94 speed ( $r^2 = 0.6$ ). The ERA5 reanalysis dataset has a good correlation with lower elevation sites in  
 95 Switzerland (Scherrer, 2020). The hourly ERA5 data and the 10 minute Plaffeien AWS data were linearly  
 96 interpolated to the 5 minute data frequency of the EP AWS.

97 Due to a power failure, all data from the EP AWS was lost from 27<sup>th</sup> February 15:20 2019 to 2<sup>nd</sup> March  
 98 15:00 2019 (equivalent to around 7% of the measurement period). During heavy snowfall events, the  
 99 ultrasonic wind sensor was blocked and recorded zero values. ERA5 was used to fill such errors and data  
 100 gaps. Near-surface humidity is not provided directly in ERA5 dataset, but from near-surface (2 m from the  
 101 surface) temperature ( $T_{ERA5}$ ) and dew point temperature ( $Tw_{ERA5}$ ) the relative humidity (RH) at 2 m  
 102 was calculated as:

$$RH = 100 \cdot \frac{e_{sat}(Tw_{ERA5})}{e_{sat}(T_{ERA5})} \quad (1)$$

103 where the saturation vapour pressure function  $e_{sat}$  is expressed with the Teten's formula (Tetens, 1930):

$$e_{sat}(T) = a_1 \cdot e^{(a_3 \cdot \frac{T}{(T+273.16-a_4)})} \quad (2)$$

104 with T in °C and the parameters set for saturation over water ( $a_1 = 611.21$  Pa,  $a_3 = 17.502$  and  $a_4 = 32.19$   
 105 K) according to Buck (1981). Zero wind speed values were recorded whenever snow accumulated on the  
 106 ultrasonic wind sensor. All such null values were replaced using the ERA5 dataset.

107 The ERA5 grid point chosen (Latitude 46° 38' 24" N, Longitude 7° 14' 24" E) for the EP site was around  
 108 9 km away from the actual site. All the ERA5 variables were therefore fitted with the EP dataset via linear  
 109 regressions. With the modified ERA5 dataset, we were also able to further extend the EP dataset and allow  
 110 the model to run beyond 18<sup>th</sup> March 2019. Precipitation was filled as null values beyond 18<sup>th</sup> March 2019.

111 2.2.1 Field Measurements for Validation  
 112 The volume was determined by decomposing the ice structure into a cylinder (length  $2R$  and height  $h$ )  
 113 and a cone (radius  $r$  and height  $(H_i - h)$ ) through the following equation:

$$V = \pi \cdot R^2 \cdot h + 1/3 \cdot \pi \cdot r^2 \cdot (H_i - h) \quad (3)$$

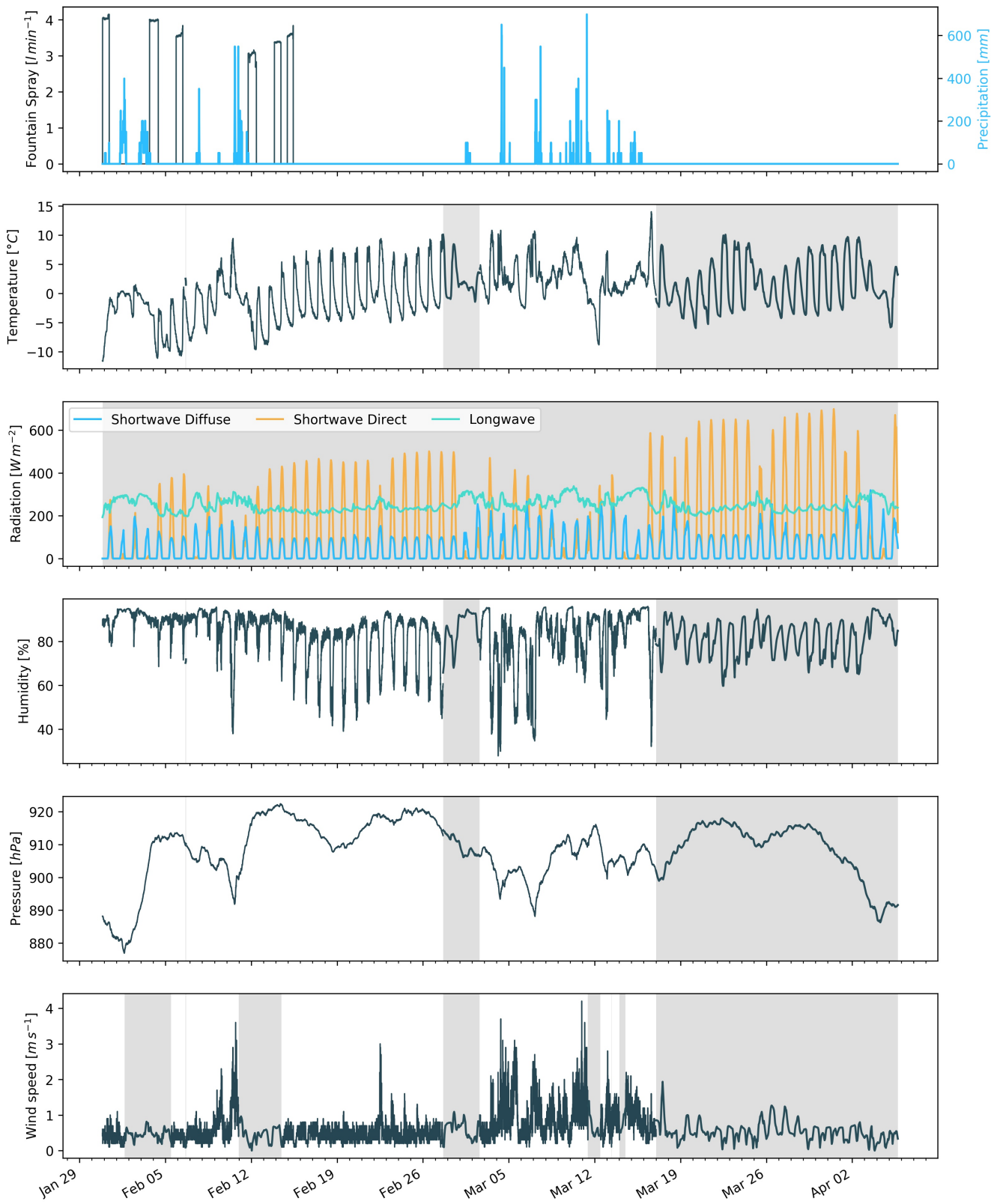


**Figure 3.** Measurements at the AWS of EP were used as main model input data in 5 minute frequency. Plaffeien AWS provided the precipitation data. Incoming shortwave and longwave radiation were obtained from ERA5 reanalysis dataset. Several data gaps and errors were also filled from the ERA5 dataset (shaded regions).

114 Manual measurements were performed at the end of the freezing period on 14<sup>th</sup> February 16:00 2019  
 115 (only one more fountain run was possible after this date) to estimate  $r, R, h, H_i, H_f$  (see Fig. 2 for the  
 116 different geometry components):

$$0.55 \leq r \leq 1m ; 1.1 \leq R \leq 1.2m ; 0.1 \leq h \leq 0.2m ; 0.6 \leq H_i \leq 0.8m ; 1.3 \leq H_f \leq 1.4m$$

117 The ranges of the variables show the variance of the Icestupa's dimensions across different compass  
 118 orientations. Correspondingly, the volume range estimated for the first validation point was  $0.857 \pm 0.186$   
 119  $m^3$  on 14<sup>th</sup> February 16:00 2019.

120 The second validation point corresponds to the end of the melting process on 10<sup>th</sup> March 18:00 2019.  
 121 Based on the webcam imagery and manual measurement, a thin layer of ice with an observed thickness  
 122 between 0.01 to 0.06 m could be quantified. This results in the volume range for the second validation to  
 123 be  $0.13 \pm 0.09 m^3$  on 11<sup>th</sup> March 2019

124 In reality, the EP ice structure was more cylindrical until a height of 0.2 m and conical afterwards until a  
 125 height of 0.6 m with a radius of 1.18 m. However, we assume a conical shape of this ice structure in order  
 126 to apply the modelling strategy described below.

### 3 MODEL SETUP

127 The model consists of three parts which calculate, a) the geometric evolution of the Icestupa, b) the energy  
 128 balance and c) the mass balance as shown schematically in Fig. 4. A bulk energy and mass balance model  
 129 is used to calculate the amounts of ice, meltwater, water vapour and runoff water of the Icestupa every 5  
 130 minutes.

#### 3.1 Icestupa geometric evolution

131 Radius  $r_{ice}^i$  and height  $h_{ice}^i$  define the dimensions of the Icestupa assuming its geometry to be a cone as  
 132 shown in Fig. 5. The surface area  $A^i$  exposed to the atmosphere and volume  $V^i$  are:

$$A = \pi \cdot r_{ice} \cdot \sqrt{r_{ice}^2 + h_{ice}^2} \quad (4)$$

$$V = \pi/3 \cdot r_{ice}^2 \cdot h_{ice} \quad (5)$$

134 Note that we do not specify the time step superscript  $i$  of the shape variables  $A, V, r_{ice}$  and  $h_{ice}$  for  
 135 brevity. The equations used henceforth display model time step superscript  $i$  only if it is different from the  
 136 current time step.

137 With the mass of the Icestupa  $M_{ice}$ , its current volume can also be expressed as:

$$V = M_{ice}/\rho_{ice} \quad (6)$$

138 where  $\rho_{ice}$  is the density of ice ( $917 kg m^{-3}$ ). The model of the Icestupa is initialised with a thickness  
 139 of  $\Delta x$  (defined in 3.2) and a circular area of radius  $r_F$ . The constant  $r_F$  represents the mean spray radius  
 140 of the fountain. This fountain spray radius is determined by modelling the projectile motion of the water

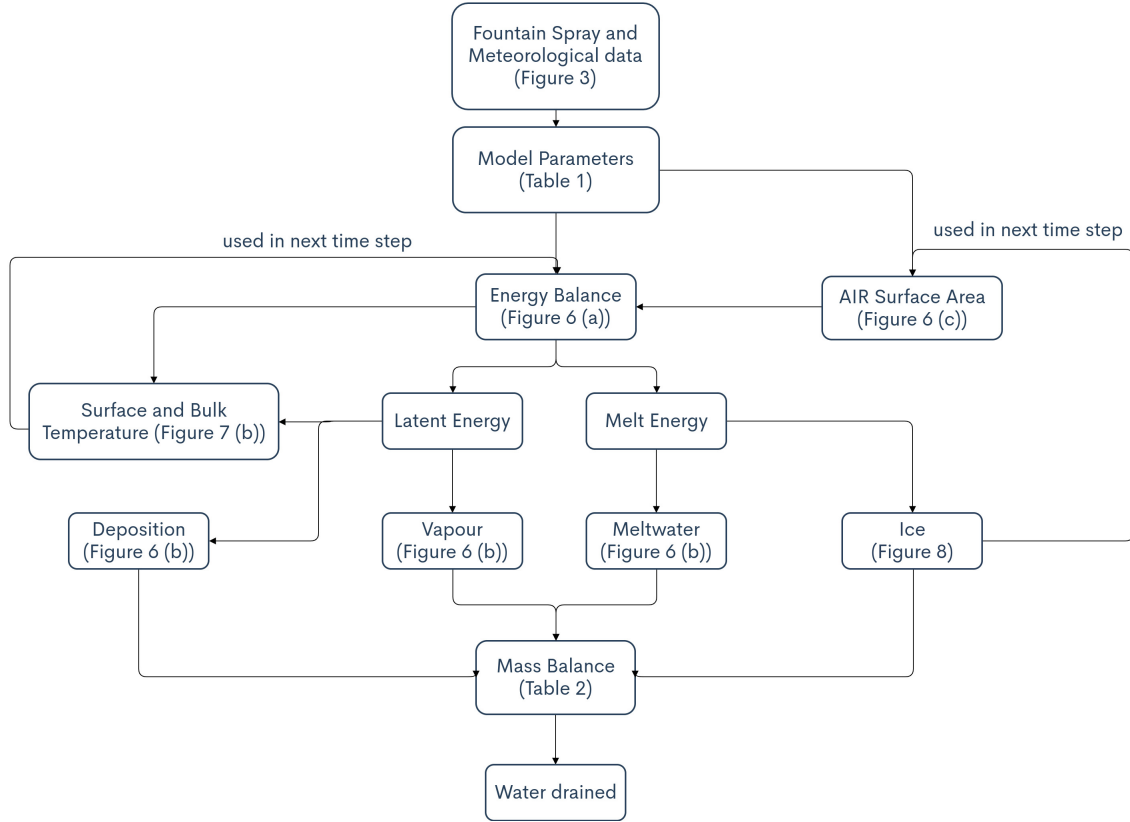


**Figure 4.** Model schematic showing the algorithm used in the model at every time step. Further details about the variables can be found in the associated tables and figures.

141 droplets. Using mass conservation, the droplet speed  $v_F$  can be determined from the spray rate  $d_F$  and the  
 142 diameter  $dia_F$  of the nozzle as follows:

$$v_F = \frac{d_F}{\pi \cdot dia_F^2 / 4} \quad (7)$$

143 Afterwards, we assume that the water droplets move with an air friction free projectile motion from  
 144 the fountain nozzle with a height  $h_F$  to the ice/ground surface. The resulting spray radius  $r_F$  was then  
 145 determined from the projectile motion equation as follows:

$$r_F = \frac{v_F \cdot \cos\theta_F (v_F \cdot \sin\theta_F + \sqrt{(v_F \cdot \sin\theta_F)^2 + 2 \cdot g \cdot h_F})}{g} \quad (8)$$

146 where  $g = 9.8 \text{ ms}^{-2}$  is the acceleration due to gravity and  $\theta_F = 45^\circ$  is the angle of launch.

147 During subsequent time steps, the dimensions of the Icestupa evolve assuming a uniform ice formation  
 148 and decay across its surface area with an invariant slope  $s_{cone} = \frac{h_{ice}}{r_{ice}}$  as shown in Fig. 5. During these time  
 149 steps, the volume is parameterised using Eqn. 5 as:

$$V = \pi / 3 \cdot r_{ice}^3 \cdot s_{cone} \quad (9)$$

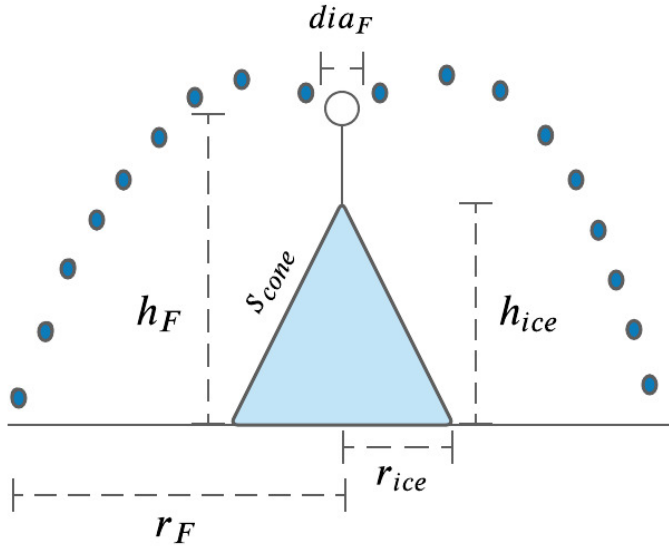


**Figure 5.** Shape variables and fountain constants of the EP Icestupa.  $r_{ice}$  is the radius,  $h_{ice}$  is the height and  $s_{cone}$  is the slope of the ice cone.  $r_F$  is the spray radius,  $h_F$  is the height and  $dia_F$  is the nozzle diameter of the fountain.

150 However, the Icestupa cannot outgrow the maximum range of the water droplets ( $(r_{ice})_{max} = r_F$ ).  
 151 Combining equations 5, 6 and 9, the geometric evolution of the Icestupa at each time step  $i$  can be  
 152 determined by considering the following rules:

$$(r_{ice}, h_{ice}) = \begin{cases} (r_F, \Delta x) & \text{if } i = 0 \\ (r_{ice}^{i-1}, \frac{3 \cdot M_{ice}}{\pi \cdot \rho_{ice} \cdot (r_{ice}^{i-1})^2}) & \text{if } r_{ice}^{i-1} \geq r_F \text{ and } \Delta M_{ice} > 0 \text{ where } \Delta M_{ice} = M_{ice}^{i-1} - M_{ice}^{i-2} \\ (\frac{3 \cdot M_{ice}}{\pi \cdot \rho_{ice} \cdot s_{cone}})^{1/3} \cdot (1, s_{cone}) & \text{otherwise} \end{cases} \quad (10)$$

### 153 3.2 Energy Balance

154 The energy balance equation (Hock, 2005) for the Icestupa is formulated as follows:

$$q_{net} = q_{SW} + q_{LW} + q_L + q_S + q_F + q_G \quad (11)$$

155 where  $q_{net}$  is the net energy flux in  $[W m^{-2}]$ ;  $q_{SW}$  is the net shortwave radiation;  $q_{LW}$  is the net longwave  
 156 radiation;  $q_L$  and  $q_S$  are the turbulent latent and sensible heat fluxes.  $q_F$  represents the heat exchange of the  
 157 fountain water droplets with the AIR ice surface during fountain on time steps.  $q_G$  represents ground heat  
 158 flux between Icestupa surface and Icestupa interior. Energy transferred in the direction of the ice surface is  
 159 always denoted as positive and away as negative.

160 Equation 11 is usually referred to as the energy budget for “the surface”, but practically it must apply to a  
 161 surface layer of ice with a finite thickness  $\Delta x$ . The energy flux acts upon the Icestupa surface layer which  
 162 has an upper and a lower boundary defined by the atmosphere and the ice body of the Icestupa, respectively.  
 163 The parameter selection for  $\Delta x$  is based on the following two arguments: (a) the ice thickness  $\Delta x$  should

164 be small enough to represent the daily surface temperature variations and (b)  $\Delta x$  should be large enough  
 165 for these temperature variations to not reach the bottom of the surface layer. Therefore, we introduced a 5  
 166 mm thick ice surface layer, over which the energy balance is calculated. A sensitivity analysis was later  
 167 performed to understand the influence of this factor. Here, we define the surface temperature  $T_{ice}$  to be  
 168 the modelled average temperature of the Icestupa surface layer and the energy flux  $q_{net}$  is assumed to act  
 169 uniformly across the Icestupa area  $A$ .

### 170 3.2.1 Net Shortwave Radiation $q_{SW}$

171 The net shortwave radiation  $q_{SW}$  is computed as follows:

$$q_{SW} = (1 - \alpha) \cdot (SW_{direct} \cdot f_{cone} + SW_{diffuse}) \quad (12)$$

172 where  $SW_{direct}$  and  $SW_{diffuse}$  are the ERA5 direct and diffuse short wave radiation,  $\alpha$  is the modelled  
 173 albedo and  $f_{cone}$  is the area fraction of the ice structure exposed to the direct shortwave radiation.

174 We model the albedo using a scheme described in Oerlemans and Knap (1998). The scheme records the  
 175 decay of albedo with time after fresh snow is deposited on the surface.  $\delta t$  records the number of time steps  
 176 after the last snowfall event. After snowfall, albedo changes over a time step,  $\delta t$ , as

$$\alpha = \alpha_{ice} + (\alpha_{snow} - \alpha_{ice}) \cdot e^{(-\delta t)/\tau} \quad (13)$$

177 where  $\alpha_{ice}$  is the bare ice albedo value (0.35),  $\alpha_{snow}$  is the snow ice albedo value (0.85) and  $\tau$  is a decay  
 178 rate, which determines how fast the albedo of the ageing snow reaches this value. The decay rate  $\tau$  is  
 179 assumed to have a base value of 10 days similar to values obtained by Schmidt et al. (2017) for wet surfaces  
 180 and its maximal value is set based on observations by Oerlemans and Knap (1998) as shown in Table 1.  
 181 Furthermore, the albedo  $\alpha$  varies depending on the water source that formed the current Icestupa surface.  
 182 Correspondingly, the albedo is reset to the value of bare ice albedo if the fountain is spraying water onto  
 183 the current ice surface and to the value of fresh snow albedo if a snowfall event occurred. Snowfall events  
 184 are assumed if the air temperature is below  $T_{ppt} = 1^{\circ}C$  (Fujita and Ageta, 2000).

185 The area fraction  $f_{cone}$  of the ice structure exposed to the direct shortwave radiation depends on the  
 186 shape considered. The direct solar radiation incident on the AIR surface is first decomposed into horizontal  
 187 and vertical components using the solar elevation angle  $\theta_{sun}$ . For a conical shape, half of the total curved  
 188 surface is exposed to the vertical component of the direct shortwave radiation and the projected triangle  
 189 of the curved surface is exposed to the horizontal component of the direct shortwave radiation. The solar  
 190 elevation angle  $\theta_{sun}$  used is modelled using the parametrisation proposed by Woolf (1968). Accordingly,  
 191  $f_{cone}$  is determined as follows:

$$f_{cone} = \frac{(0.5 \cdot r_{ice} \cdot h_{ice}) \cdot \cos\theta_{sun} + (\pi \cdot r_{ice}^2 / 2) \cdot \sin\theta_{sun}}{\pi \cdot r_{ice} \cdot (r_{ice}^2 + h_{ice}^2)^{1/2}} \quad (14)$$

192 The ERA5 diffuse shortwave radiation is assumed to impact the conical Icestupa surface uniformly.

### 193 3.2.2 Net Longwave Radiation $q_{LW}$

194 The net longwave radiation  $q_{LW}$ , for which there were no direct measurements available at EP, is  
 195 determined as follows:

$$q_{LW} = LW_{in} - \sigma \cdot \epsilon_{ice} \cdot (T_{ice} + 273.15)^4 \quad (15)$$

where  $T_a$  represents the measured air temperature,  $T_{ice}$  is the modelled surface temperature, both temperatures are given in  $^{\circ}\text{C}$ ,  $\sigma = 5.67 \cdot 10^{-8} \text{ J m}^{-2} \text{ s}^{-1} \text{ K}^{-4}$  is the Stefan-Boltzmann constant,  $LW_{in}$  denotes the incoming longwave radiation derived from the ERA5 dataset and  $\epsilon_{ice}$  is the corresponding emissivity value for the Icestupa surface (see Table 1).

### 3.2.3 Turbulent sensible $q_S$ and latent $q_L$ heat fluxes

The turbulent sensible  $q_S$  and latent heat  $q_L$  fluxes are computed with the following expressions proposed by Garratt (1992):

$$q_S = c_a \cdot \rho_a \cdot p_a / p_{0,a} \cdot \frac{\kappa^2 \cdot v_a \cdot (T_a - T_{ice})}{(\ln \frac{h_{AWS}}{z_{ice}})^2} \quad (16)$$

$$q_L = 0.623 \cdot L_s \cdot \rho_a / p_{0,a} \cdot \frac{\kappa^2 \cdot v_a (p_{v,a} - p_{v,ice})}{(\ln \frac{h_{AWS}}{z_{ice}})^2} \quad (17)$$

where  $h_{AWS}$  is the measurement height above the ground surface of the AWS (in  $m$ ),  $v_a$  is the wind speed in  $\text{m s}^{-1}$  and  $M_F$  denotes fountain water spray mass in  $\text{kg}$ .  $c_a$  is the specific heat of air at constant pressure ( $1010 \text{ J kg}^{-1} \text{ K}^{-1}$ ),  $\rho_a$  is the air density at standard sea level ( $1.29 \text{ kg m}^{-3}$ ),  $p_{0,a}$  is the air pressure at standard sea level ( $1013 \text{ hPa}$ ),  $\kappa$  is the von Karman constant (0.4),  $L_s$  is the heat of sublimation ( $2848 \text{ kJ kg}^{-1}$ ) and  $z_{ice}$  (1.7 mm) denotes the roughness length of ice (momentum and scalar) described in (Garratt, 1992). The vapor pressures over air ( $p_{v,a}$ ) and ice ( $p_{v,ice}$ ) was obtained using the following formulation given in WMO (2018):

$$\begin{aligned} p_{v,a} &= 6.107 \cdot 10^{(7.5 \cdot T_a / (T_a + 237.3))} \\ p_{v,ice} &= (1.0016 + 3.15 \cdot 10^{-6} \cdot p_a - 0.074 \cdot p_a^{-1}) \cdot (6.112 \cdot e^{(22.46 \cdot T_{ice} / (T_{ice} + 272.62))}) \end{aligned} \quad (18)$$

where  $p_a$  is the measured air pressure in  $\text{hPa}$ .

### 3.2.4 Fountain water heat flux $q_F$

The total energy flux is further influenced through the heat flux caused by the water that was additionally added to the surface of the Icestupa during the time the fountain was running. We take this interaction between the fountain water and the ice surface into account by assuming that the ice surface temperature remains constant at  $0^{\circ}\text{C}$  during time steps when the fountain is active. This process can be divided into two simultaneous steps: (a) the water temperature  $T_{water}$  is cooled to  $0^{\circ}\text{C}$  and (b) the ice surface temperature is warmed to  $0^{\circ}\text{C}$ . Process (a) transfers the necessary energy for process (b) throughout the fountain runtime. We further assume that this process is instantaneous, i.e. the ice temperature is immediately set to  $0^{\circ}\text{C}$  within just one time step  $\Delta t$  when the fountain is switched on. Thus, the heat flux caused by the fountain water is calculated as follows:

$$q_F = \begin{cases} 0 & \text{if } \Delta M_F = 0 \\ \frac{\Delta M_F \cdot c_{water} \cdot T_{water}}{\Delta t \cdot A} + \frac{\rho_{ice} \cdot \Delta x \cdot c_{ice} \cdot T_{ice}}{\Delta t} & \text{if } \Delta M_F > 0 \end{cases} \quad (19)$$

221 with  $c_{ice}$  as the specific heat of ice.

### 222 3.2.5 Bulk Icestupa heat flux $q_G$

223 The bulk Icestupa heat flux  $q_G$  corresponds to the ground heat flux in normal soils and is caused by the  
224 temperature gradient between the surface layer ( $T_{ice}$ ) and the ice body ( $T_{bulk}$ ). It is expressed by using the  
225 heat conduction equation as follows:

$$q_G = k_{ice} \cdot (T_{bulk} - T_{ice}) / l_{ice} \quad (20)$$

226 where  $k_{ice}$  is the thermal conductivity of ice ( $2.123 \text{ W m}^{-1} \text{ K}^{-1}$ ),  $T_{bulk}$  is the mean temperature of the  
227 ice body within the Icestupa and  $l_{ice}$  is the average distance of any point in the surface to any other point in  
228 the ice body.  $T_{bulk}$  is initialised as  $0^\circ\text{C}$  and later determined from Eqn. 20 as follows:

$$T_{bulk}^{i+1} = T_{bulk} - (q_G \cdot A \cdot \Delta t) / (M_{ice} \cdot c_{ice}) \quad (21)$$

229 Since we assume a conical shape with  $r_{ice} > h_{ice}$ ,  $l_{ice}$  cannot be greater than  $2r_{ice}$  and also cannot  
230 be less than  $\Delta x$ . Therefore, the average distance from any point on the surface to any point inside is  
231  $\Delta x \leq l_{ice} \leq r_{ice}$ . We calculate  $q_G$  here assuming  $l_{ice} = r_{ice}/2$ .

### 232 3.2.6 Surface temperature changes and melt energy $q_{melt}$

233 The available net energy  $q_{net}$  partly increases surface temperature, but also contributes to ice melt at the  
234 surface of the Icestupa.  $q_T$  denotes the energy used on changing the surface temperature  $T_{ice}$  and  $q_{melt}$   
235 denotes the energy used to produce meltwater. So Eqn. 11 can be rewritten as:

$$q_{net} = q_{melt} + q_T \quad (22)$$

236 We define the freezing energy as  $q_{freeze} = (q_{net} - q_L)$ . This is because the latent heat always contributes  
237 to temperature fluctuations. Now, the temperature fluctuates based on three scenarios, namely (1) the  
238 freezing energy flux is negative but cannot freeze all the fountain water output; (2) the freezing energy flux  
239 is negative and can freeze all the fountain water output; (3) the freezing energy is positive or the fountain is  
240 inactive ( $\Delta M_F = 0$ ). Therefore, we express the rate of change of temperature as follows:

$$\frac{\Delta T}{\Delta t} = \begin{cases} -T_{ice}^{i-1} / \Delta t & \text{if } q_{freeze} < 0 \text{ and } \Delta M_F \geq -q_{freeze} \cdot A \cdot \Delta t / L_f \\ (\Delta M_F \cdot L_f) / (\rho_{ice} \cdot c_{ice} \cdot \Delta x \cdot A \cdot \Delta t) & \text{if } q_{freeze} < 0 \text{ and } \Delta M_F < -q_{freeze} \cdot A \cdot \Delta t / L_f \\ q_{net} / (\rho_{ice} \cdot c_{ice} \cdot \Delta x) & \text{if } \Delta M_F = 0 \text{ or } q_{freeze} > 0 \end{cases} \quad (23)$$

241 Whenever the model predicts  $T_{ice}^{i+1} > 0^\circ\text{C}$ , then the surface temperature is set to  $0^\circ\text{C}$  in the corresponding  
242 time step and additional energy contributes to  $q_{melt}$ . Combining these requirements, we get:

$$(q_T, q_{melt}) = \begin{cases} (\rho_{ice} \cdot c_{ice} \cdot \Delta x \cdot \frac{\Delta T}{\Delta t}, q_{net} - q_L - \rho_{ice} \cdot c_{ice} \cdot \Delta x \cdot \frac{\Delta T}{\Delta t}) & \text{if } T_{ice}^{i+1} \leq 0^\circ\text{C} \text{ and } \Delta M_F > 0 \\ (\rho_{ice} \cdot c_{ice} \cdot \Delta x \cdot \frac{\Delta T}{\Delta t}, q_{net} - \rho_{ice} \cdot c_{ice} \cdot \Delta x \cdot \frac{\Delta T}{\Delta t}) & \text{if } T_{ice}^{i+1} \leq 0^\circ\text{C} \text{ and } \Delta M_F = 0 \\ (-\rho_{ice} \cdot c_{ice} \cdot \Delta x \cdot \frac{T_{ice}^i}{\Delta t}, q_{net} - q_L + \rho_{ice} \cdot c_{ice} \cdot \Delta x \cdot \frac{T_{ice}^i}{\Delta t}) & \text{if } T_{ice}^{i+1} > 0^\circ\text{C} \text{ and } \Delta M_F > 0 \\ (-\rho_{ice} \cdot c_{ice} \cdot \Delta x \cdot \frac{T_{ice}^i}{\Delta t}, q_{net} + \rho_{ice} \cdot c_{ice} \cdot \Delta x \cdot \frac{T_{ice}^i}{\Delta t}) & \text{if } T_{ice}^{i+1} > 0^\circ\text{C} \text{ and } \Delta M_F = 0 \end{cases} \quad (24)$$

**Table 1.** Free parameters in the model categorised as constant, uncertain and site parameters. Base value (B) and uncertainty (U) were taken from the literature. For assumptions (assum.), the uncertainty was chosen to be relatively large (5 %). For measurements (meas.), the uncertainty due to parallax errors is chosen to be (1 %).

Constant Parameters	Symbol	Value	References
Van Karman constant	$\kappa$	0.4	B: Cuffey and Paterson
Stefan Boltzmann constant	$\sigma$	$5.67 \cdot 10^{-8} W m^{-2} K^{-4}$	B: Cuffey and Paterson
Air pressure at sea level	$p_{0,a}$	1013 hPa	B: Mölg and Hardy
Density of water	$\rho_w$	$1000 kg m^{-3}$	B: Cuffey and Paterson
Density of ice	$\rho_{ice}$	$917 kg m^{-3}$	B: Cuffey and Paterson
Density of air	$\rho_a$	$1.29 kg m^{-3}$	B: Mölg and Hardy
Specific heat of water	$c_w$	$4186 J kg^{-1} ^\circ C^{-1}$	B: Cuffey and Paterson
Specific heat of ice	$c_{ice}$	$2097 J kg^{-1} ^\circ C^{-1}$	B: Cuffey and Paterson
Specific heat of air	$c_a$	$1010 J kg^{-1} ^\circ C^{-1}$	B: Mölg and Hardy
Thermal conductivity of ice	$k_{ice}$	$2.123 W m^{-1} K^{-1}$	B: Bonales et al.
Latent Heat of Sublimation	$L_s$	$2848 kJ kg^{-1}$	B: Cuffey and Paterson
Latent Heat of Evaporation	$L_e$	$2514 kJ kg^{-1}$	B: Cuffey and Paterson
Latent Heat of Fusion	$L_f$	$334 kJ kg^{-1}$	B: Cuffey and Paterson
Gravitational acceleration	$g$	$9.81 m s^{-2}$	B: Cuffey and Paterson
Uncertain Parameters		Range	
Precipitation	$T_{ppt}$	$1 ^\circ C$	$\pm 1 ^\circ C$
Temperature threshold			B + U: Fujita and Ageta, Zhou et al.
Ice Emissivity	$\epsilon_{ice}$	0.95	[0.949,0.993] B: Cuffey and Paterson; U: Hori et al.
Ice Albedo	$\alpha_{ice}$	0.35	$\pm 5 \%$ B: Cuffey and Paterson; U: assum.
Snow Albedo	$\alpha_{snow}$	0.85	$\pm 5 \%$ B: Cuffey and Paterson; U: assum.
Albedo Decay Rate	$\tau$	10 days	[1, 22] days B: Schmidt et al.; U: Oerlemans and Knap assum.
Ice layer thickness	$\Delta x$	5 mm	[1, 10] mm
Site Parameters			
Fountain diameter	nozzle	$dia_F$	5 mm $\pm 1 \%$ B: meas. ; U: assum.
Fountain height		$h_F$	$\pm 1 \%$ B: meas. ; U: assum.
Fountain temperature	water	$T_{water}$	$[0, 9] ^\circ C$ B: meas. ; U: meas.
AWS height		$h_{AWS}$	$\pm 1 \%$ B: meas. ; U: assum.

243 **3.3 Mass Balance**

244 The mass balance equation is used to derive the water that drains away ( $M_{runoff}$ ) as follows:

$$\frac{\Delta M_{runoff}}{\Delta t} = \frac{\Delta M_F + \Delta M_{ppt} + \Delta M_{dpt} - \Delta M_{ice} - \Delta M_{melt} - \Delta M_{vapour}}{\Delta t} \quad (25)$$

245 where  $\Delta M = M^i - M^{i-1}$ . Here  $\frac{\Delta M_F}{\Delta t} = d_F$  where  $d_F$  is the spray of the fountain measured in  $[kg s^{-1}]$ ;  
 246  $M_{ppt}$  is the cumulative precipitation and  $M_{dpt}$  is the cumulative accumulation through water vapour  
 247 condensation or deposition;  $M_{ice}$  is the cumulative mass of ice;  $M_{melt}$  is the cumulative mass of melt water  
 248 and  $M_{vapour}$  represents the cumulative water vapor loss by evaporation or sublimation.

249 Precipitation input is calculated as:

$$\frac{\Delta M_{ppt}}{\Delta t} = \begin{cases} \pi \cdot r_{ice}^2 \cdot \rho_w \cdot ppt & \text{if } T_a < T_{ppt} \\ 0 & \text{if } T_a \geq T_{ppt} \end{cases} \quad (26)$$

250 where  $\rho_w$  is the density of water ( $1000 kg m^{-3}$ ),  $ppt$  is the measured precipitation rate in  $[m s^{-1}]$  and  
 251  $T_{ppt}$  is the temperature threshold below which precipitation falls as snow. Here, snowfall events were  
 252 identified using  $T_{ppt}$  as  $1^\circ C$ . Snow mass input is calculated by assuming a uniform deposition over the  
 253 entire circular footprint of the Icestupa.

254 The latent heat flux is used to estimate either the evaporation and condensation processes or sublimation  
 255 and deposition processes. To differentiate between these two possibilities, we classify the time steps into  
 256 humid or non-humid depending on whether the corresponding relative humidity value is above or below  
 257 60% (Stigter et al., 2018). On humid time steps, we assume condensation or evaporation to occur whereas  
 258 on non-humid time steps deposition or sublimation can occur. Correspondingly, latent heat of evaporation  
 259 ( $L_e$ ) is used for humid time steps and latent heat of sublimation ( $L_s$ ) is used for non-humid time steps.  
 260 Water accumulation and vapour loss from the Icestupa surface is calculated as follows:

$$\left( \frac{\Delta M_{vapour}}{\Delta t}, \frac{\Delta M_{dpt}}{\Delta t} \right) = \begin{cases} (-q_L \cdot A/L, 0) & \text{if } q_L < 0 \\ (0, q_L \cdot A/L) & \text{if } q_L \geq 0 \end{cases} \quad (27)$$

261 where  $L = \begin{cases} L_s & \text{if } RH < 60 \\ L_e & \text{if } RH \geq 60 \end{cases}$

262 Using the melt energy  $q_{melt}$ , we estimate the frozen and melted ice mass ( $\Delta M_{ice}$ ,  $\Delta M_{melt}$ ). Removing  
 263 the contribution of precipitation and combining Eqn. 27 we are left with the contribution from the melt  
 264 energy as follows:

**Table 2.** Summary of mass balance components for the EP experiment after the fountain spray was stopped (on 15<sup>th</sup> February 2019) and at the end of the model run (on 5<sup>th</sup> April). All parameters except  $M_F$  were modelled.

	Mass Component	Fountain spray ends	Model ends
Input	$M_F$	18060 kg	18060 kg
	$M_{ppt}$	438 kg	461 kg
	$M_{dpt}$	7 kg	33 kg
Output	$M_{melt}$	154 kg	1005 kg
	$M_{ice}$	808 kg	0 kg
	$M_{vapour}$ $M_{runoff}$	11 kg 17532 kg	16 kg 17532 kg

$$\left( \frac{\Delta M_{ice} - \Delta M_{ppt} - \Delta M_{dpt} + \Delta M_{vapour}}{\Delta t}, \frac{\Delta M_{melt}}{\Delta t} \right) \text{ if } RH < 60 \\ \left( \frac{\Delta M_{ice} - \Delta M_{ppt} - \Delta M_{dpt}}{\Delta t}, \frac{\Delta M_{melt} + \Delta M_{vapour}}{\Delta t} \right) \text{ if } RH \geq 60 \right\} = \begin{cases} \frac{q_{melt} \cdot A}{L_f} \cdot (-1, 1) & \text{if } q_{melt} \geq 0 \\ \frac{q_{melt} \cdot A}{L_f} \cdot (-1, 0) & \text{if } q_{melt} < 0 \text{ and } \frac{\Delta M_F}{\Delta t} \geq -\frac{q_{melt} \cdot A}{L_f} \\ (\frac{\Delta M_F}{\Delta t}, 0) & \text{if } q_{melt} < 0 \text{ and } 0 \leq \frac{\Delta M_F}{\Delta t} < -\frac{q_{melt} \cdot A}{L_f} \end{cases} \quad (28)$$

265 Now, with all the other terms known in Eqn. 25, the water drainage/runoff can be determined.

266 Considering AIRs as water reservoirs, we can quantify their potential through the amount of water they  
267 store (storage quantity) and the length of time they store it (storage duration). Another means of comparing  
268 different Icestupas is through their water storage efficiency defined accordingly as:

$$\text{Storage Efficiency} = \frac{M_{melt}}{(M_F + M_{ppt} + M_{dpt})} \cdot 100 \quad (29)$$

## 4 MODEL RESULTS

269 The model was forced with meteorological data from 30<sup>th</sup> January to 5<sup>th</sup> April 2019 (Fig. 3) and various  
270 parameters (see Table 1) to calculate the mass and energy balance of the Icestupa.

### 4.1 Energy and mass balance calculation

272 Daily averages of some components of the energy balance are shown in Fig. 6 (b). On average during  
273 the experiment duration, the total energy balance was almost zero. Net shortwave radiation ( $32 \text{ W m}^{-2}$ ),  
274 sensible ( $9 \text{ W m}^{-2}$ ) and latent heat flux ( $2 \text{ W m}^{-2}$ ) with a mostly positive flux towards the surface of the  
275 icestupa were compensated by the net longwave radiation ( $-32 \text{ W m}^{-2}$ ) and the melt energy ( $-12 \text{ W m}^{-2}$ ).  
276 The contributions of other fluxes were negligible in comparison.

277 Net shortwave radiation is the main input to, and the most varying energy flux on the ice surface. Its  
278 variability is controlled by the surface albedo  $\alpha$  and the area fraction  $f_{cone}$  which therefore represent key

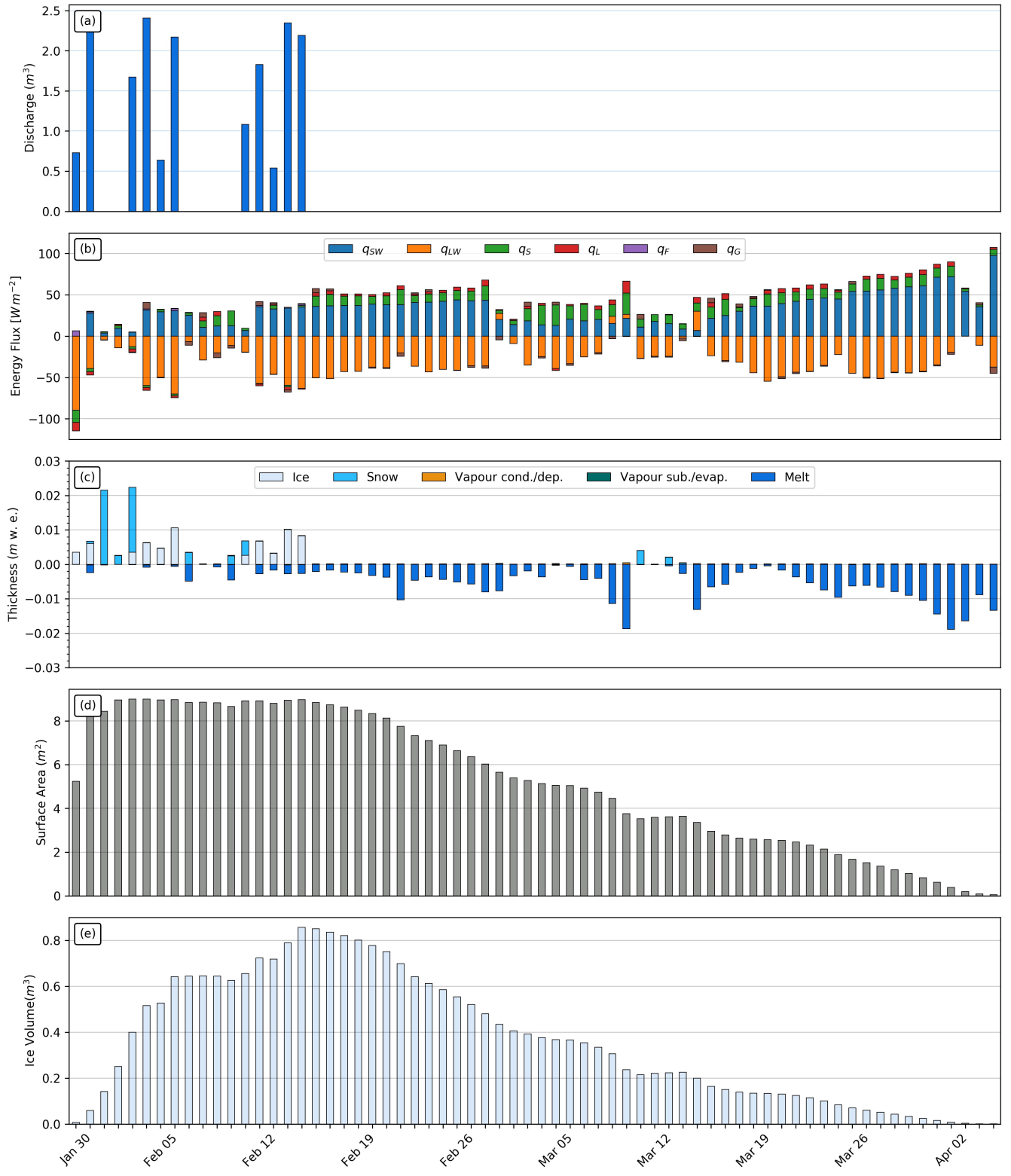


**Figure 6.** (a) Fountain discharge (b) energy flux components, (c) mass flux components (d) surface area and (e) volume of the Icestupa in daily time steps.  $q_{SW}$  is the net shortwave radiation;  $q_{LW}$  is the net longwave radiation;  $q_L$  and  $q_S$  are the turbulent latent and sensible heat fluxes.  $q_F$  represents the interactions of the ice-water boundary during fountain on time steps.  $q_G$  quantifies the heat conduction process between the Icestupa surface layer and the ice body.

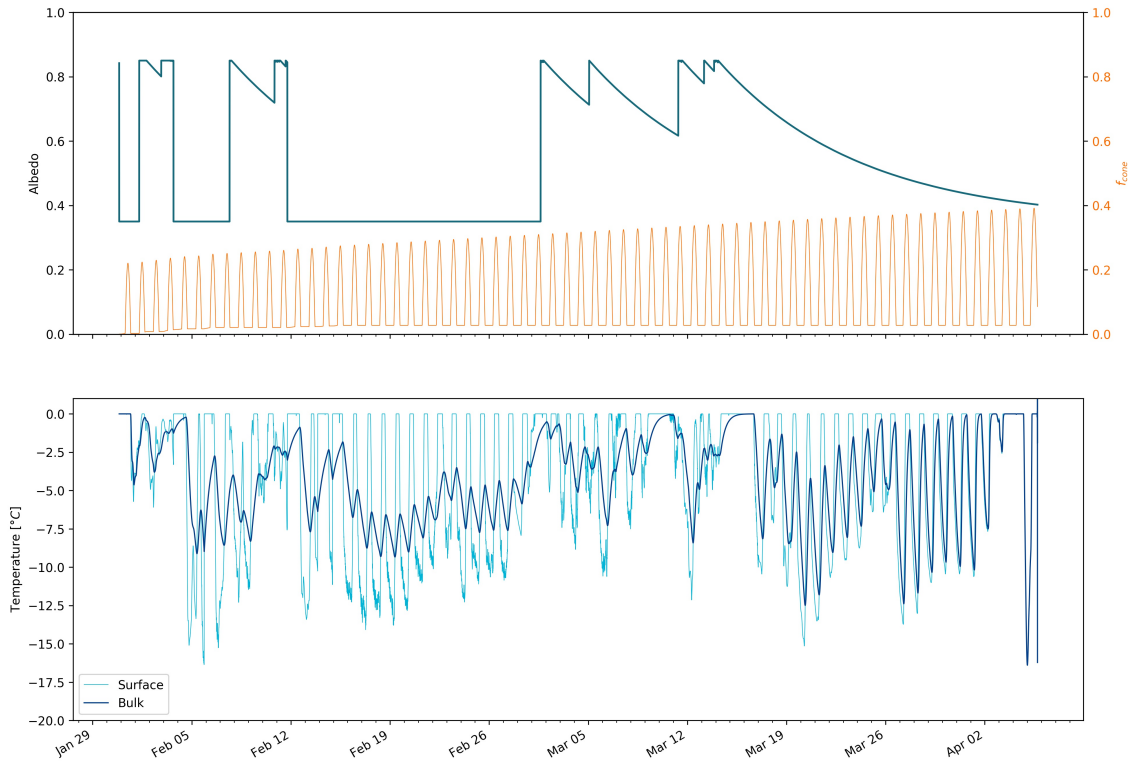


**Figure 7.** Some derived parameters of the model, namely, albedo and  $f_{cone}$  (a), Surface and bulk temperature (b). In (a), the green curve shows how snow and fountain-on events reset albedo between ice albedo and snow albedo. The decay of the snow albedo to ice albedo can also be observed. The orange curve shows how the solar radiation area fraction varied diurnally with variations in the solar elevation angle. In (b), the surface temperature (light blue curve) was forced to be  $0\text{ }^{\circ}\text{C}$  during fountain activity. The corresponding bulk temperature is shown with the dark blue curve.

variables in the energy balance (Fig. 7 (b)). Although global radiation flux reached a daily maximum value of  $339\text{ }Wm^{-2}$ ,  $q_{SW}$  only went up to  $98\text{ }Wm^{-2}$ . This is caused by the fact that only about 30 % of the direct solar radiation influenced the Icestupa surface as shown by the area fraction  $f_{cone}$  in Fig. 7 (a). Snowfall is the atmospheric variable connected most closely and proportionally to albedo. Higher and/or more frequent snowfall thus decreases the energy available for melt due to the corresponding increase in  $\alpha$ .

$q_{LW}$  was predominantly negative indicating that this energy balance component drove the freezing of the ice structure. Daily values of  $q_{LW}$  ranged from  $-90$  to  $23\text{ }Wm^{-2}$ . Turbulent sensible heat flux  $q_S$  contributed mostly to the melt of the ice structure. Daily values of  $q_S$  ranged from  $-15$  to  $26\text{ }Wm^{-2}$ . Deposition/condensation was favored over evaporation/sublimation so the mean of the turbulent latent heat flux  $q_L$  across model runtime was positive. Daily values of  $q_L$  ranged from  $-10$  to  $14\text{ }Wm^{-2}$ . Therefore, the Icestupa gained mass cumulatively from the atmosphere due to the deposition/condensation process. Fountain water heat flux  $q_F$  had a mean of zero as it was only nonzero during 1002 time steps or around 100 hours. Daily values of  $q_F$  ranged from  $-1$  to  $7\text{ }Wm^{-2}$ . The contribution of heat flux by conduction  $q_G$  was also minimal as it only varied between  $-7$  to  $8\text{ }Wm^{-2}$  with a mean of  $0\text{ }Wm^{-2}$ . The energy contributing to surface temperature changes ( $q_T$ ) was insignificant in comparison to the energy spent on freezing and melting ( $q_{melt}$ ). The resulting bulk temperature and the surface temperature are shown in Fig. 7 (b). For the total considered period,  $q_{LW}$  accounted for 32.5% of overall energy turnover. The energy turnover is

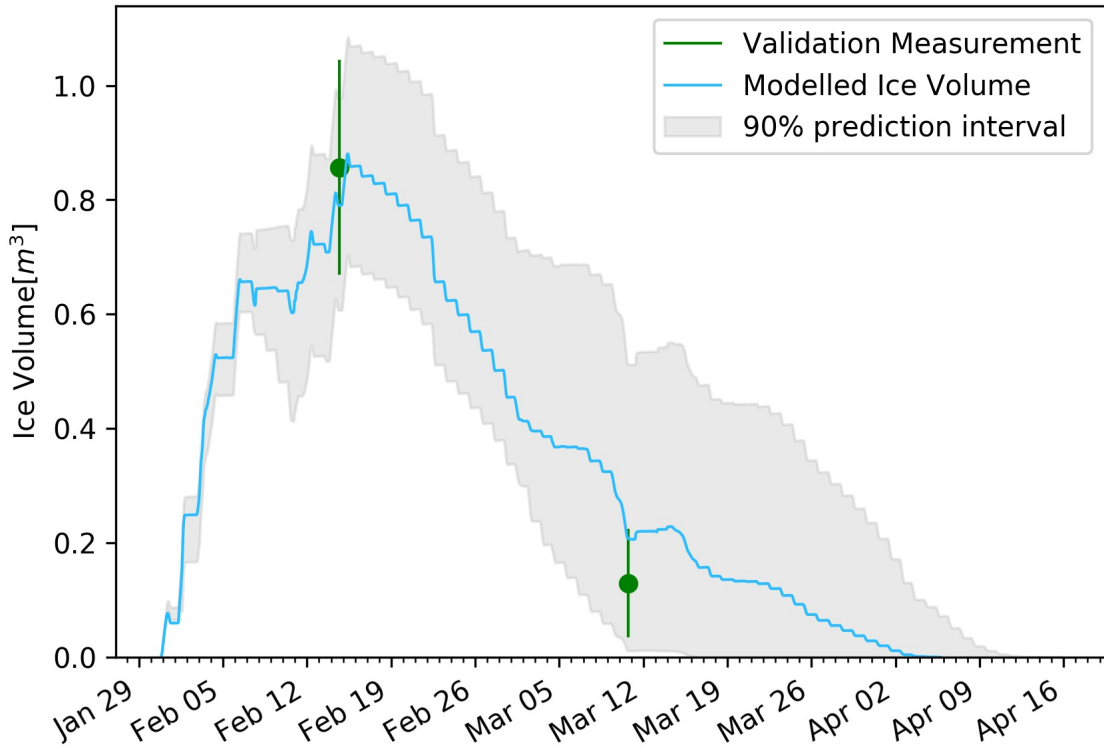


**Figure 8.** Modelled ice volume during the lifetime of the EP Icestupa (blue curve). Green line segments indicate the first and second validation measurements. The prediction interval is based on the ice volume uncertainty caused by the most sensitive parameters, namely, temperature threshold below which precipitation falls as snow and the ice emissivity.

296 calculated as the sum of energy fluxes in absolute values.  $q_{SW}$  accounted for 31.5%, followed by  $q_{melt}$   
 297 (20%),  $q_S$  (9.8%),  $q_L$  (3.2%),  $q_G$  (2%),  $q_F$  (0.2%) and  $q_T$  (0.4%).

298 Fig. 6 (c) represents the mass fluxes associated with these energy exchanges expressed in  $m$  w.e. It  
 299 shows the ice and meltwater formed due to  $q_{melt}$ , snow accumulated due to precipitation, water vapour  
 300 deposition/condensation and sublimation/evaporation due to  $q_L$ . Growth rate ( $\frac{\Delta M_{ice}}{\Delta t}$ ) shows a strong  
 301 correlation with net energy flux ( $r^2 = 0.31$ ) but poor correlation with Icestupa surface area ( $r^2 = 0.03$ ).  
 302 This is because the variance in growth rate is mostly due to the variance in  $q_{net}$  as illustrated in Fig. 6.  
 303 Since  $r_{ice}$  was initialised with the spray radius  $r_F$ , the surface area maintains a maximum initially until the  
 304 energy flux becomes positive. This trend favours the positive over the negative thickness changes resulting  
 305 in a steep increase and gradual melting of ice volume as can be seen in Fig. 8.

306 The total water used for the Icestupa development includes contributions from the fountain (97.3%),  
 307 snowfall (2.5 %) and deposition/condensation (0.2 %) as shown in Table 2. The maximum ice mass during  
 308 the whole measurement period was 806 kg, which occurred after the last fountain run on Feb 16<sup>th</sup> 2019  
 309 in the morning. Therefore, in the case of EP we used a water input of 18,560 kg, with a resultant storage  
 310 efficiency of only 5.4 %.

## 5 MODEL SENSITIVITY AND UNCERTAINTY ANALYSIS

311 The icestupa model can be regarded as a function  $f(x_1, x_2 \dots, x_n) = (y_1, y_2 \dots, y_m)$ , where  
 312  $(x_1, x_2 \dots, x_n)$  are the model parameters and  $(y_1, y_2 \dots, y_m)$  are the model outputs. The influence of each

parameter on the output variables of interest were quantified and the most important physical parameters for the subsequent uncertainty analysis were determined. The sensitivity of a parameter  $x_j$  is determined by keeping all other parameters  $x_i, i \neq j$  fixed at their baseline value and varying  $x_j$  within values that are physically plausible.

A sensitivity study on the parameters (listed in Table 1) was performed with the maximum ice volume as the target variable. All the parameters were assumed to be independent of each other with a uniform distribution. This assumption ignores the auto-correlation present among the parameters associated with the albedo parameterisation. The range of uncertain parameters were set based on available literature values or varied  $\pm 5\%$  from the base value if no such reference was available. The uncertainty of all the site parameters were caused due to parallax errors during manual measurement. This was quantified with a range of  $\pm 1\%$  from the base value. However, it must be kept in mind that, even though intended to be as objective as possible, the selection of a parameter range has a subjective part that influences the results and conclusions obtained in this analysis. The variation of the model outputs  $y_k$  is evaluated to quantify the local sensitivities  $s_{j,k}$  that are defined here as the 95% range of the simulated outputs.

To perform the uncertainty analysis, we included only parameters that influence the maximum ice volume by at least  $0.1 m^3$ . All other parameters were fixed at their baseline value. Fig. 9 shows all the variance produced by these uncertain parameters in maximum ice volume calculation. It shows that  $\epsilon_{ice}$  and  $T_{ppt}$  are the only parameters with a maximal sensitivity of more than  $0.1 m^3$  for the maximum ice volume estimate. Consequently, all other parameters were excluded from the subsequent uncertainty analysis.

The temperature threshold below which precipitation falls as snow ( $T_{ppt}$ ) was found to be the most sensitive parameter. It is used in the model to reset the albedo to snow albedo and determine snow precipitation events. The lower  $T_{ppt}$  parameter the higher the albedo (as the Icestupa surface has a lower albedo when ice-covered than when snow-covered). The variation of  $T_{ppt}$  by  $\pm 1^\circ C$  caused maximum ice volume variation of  $0.83 \pm 0.2 m^3$ .

Ice emissivity was also found to be a sensitive parameter. The higher the ice emissivity the larger the maximum ice volume as the emitted longwave radiation increases with ice emissivity. Variation of  $\epsilon_{ice}$  by 5% caused a maximum ice volume range from  $0.98 \pm 0.1 m^3$ .

In total, the sensitivity analysis required 120 simulations, and the uncertainty analysis a total of 32 simulations.

## 6 DISCUSSION

### 6.1 Model validation quality

We first evaluate the model against the validation measurements at the EP site. The uncalibrated model is able to capture both the freezing and the melting process sufficiently well as the modelled ice volume lies within the uncertainty of both validation measurements. Furthermore, the validation measurements fit well within the estimated model uncertainty. However, since this validation is based on only two points, it does limit the confidence in the model results. Even though the model estimates validate well with the ice volume, the same is not the case for the surface area. The surface area estimated from the first validation measurement is just around  $4 m^2$ , roughly half the model estimated surface area. However, the validation surface area estimate again underestimates the surface area as the actual surface area in contact with the atmosphere could have been amplified by the inherent roughness of the ice surface. Another major cause of this discrepancy was the conical shape assumption, as in reality, the Icestupa shape ranged between a cone and a cylinder (Fig. 2). The sensitivity of the model results to these errors was further amplified due to the

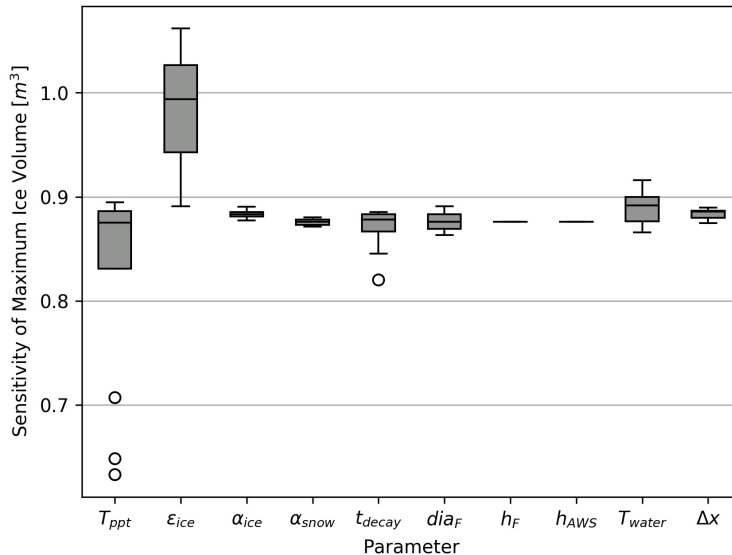


**Figure 9.** Sensitivities of maximum ice volume to all the uncertain and site parameters used in the model (Table 1). Outliers in the bar plot are shown as 'o'.

354 relatively small volume of the EP Icestupa. In summary, better and frequent validation measurements on a  
 355 **6.2 Important assumptions** have increased confidence on the model results.  
 356  
 357 In the sensitivity and uncertainty analysis presented above, we did not account for several general  
 358 assumptions and parametrisation choices that may cause model errors. Some assumptions and their  
 359 potential to cause errors are discussed below.

- 360 • Turbulent Sensible and Latent Heat Fluxes: The method used to calculate the turbulent heat fluxes  
 361 by Garratt (1992) assumes that the turbulent heat fluxes are acting over a uniform planar surface to  
 362 determine the roughness length. Since our application is on a conical surface, the distance to the ice  
 363 surface is not uniform and well defined. Hence,  $z_{ice}$  has no real physical significance here.
- 364 • Droplet flight time loss: Water losses during the flight time of fountain droplets were neglected making  
 365 all the fountain spray available for freezing. For the EP experiment, inclusion of this parameter does  
 366 not influence results since it is already accounted for in the runoff water discharge rate which was at  
 367 least  $3 \text{ l min}^{-1}$ .
- 368 • Nucleation of droplets: Corresponding to droplet flight time, ice/snow formation is also possible before  
 369 surface contact if nucleation occurs during flight time. For the EP experiment, this process will further  
 370 increase the freeze rate and hence the storage efficiency. This process is neglected for model simplicity.
- 371 • Shape Effects: The suppression of heat exchange between the snow/ice surface and the air adjacent  
 372 to the surface effectively slows down snow/ice ablation in spring and promotes the stagnation of the  
 373 cold air within topographical depressions (Fujita et al., 2010). The quantitative contribution of the  
 374 atmospheric decoupling over melting snow/ice for the total mass and energy balance is ignored in the  
 375 model.

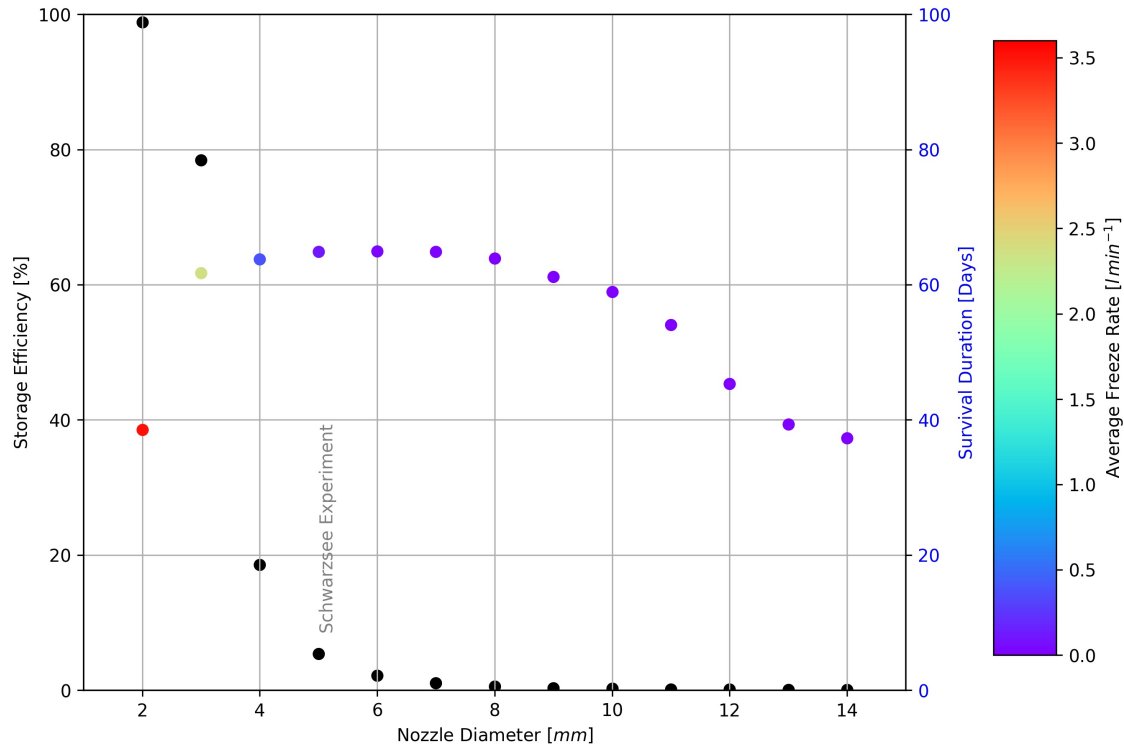


**Figure 10.** Variation in storage efficiency (black dots) and storage duration (coloured dots) with changes in fountain nozzle's nozzle diameter. The dot colours represent average freeze rate based on the color bar.

### 376 6.3 Schwarzsee vs Leh Icestupa

377 It could be argued that the relatively small EP Icestupa cannot be compared with the much larger Icestupas  
 378 in Ladakh which store millions of litres of water for several months (see Appendix 8.1). However, this is  
 379 the only Icestupa dataset currently available for such a model validation.

380 Table 2 clearly shows that for our EP experiment most of the input water (94.5 %) simply drained away  
 381 ( $M_{runoff}$ ). This high water loss through drainage is due to the fact that the average spray rate of the fountain  
 382 ( $(\frac{\Delta M_F}{\Delta t})_{mean} = 3.6 \text{ l min}^{-1}$ ) far exceeded the max Icestupa growth rate ( $(\frac{\Delta M_{ice}}{\Delta t})_{max} = 0.9 \text{ l min}^{-1}$  (w.e.)  
 383 ).

384 In the city of Leh, Ladakh at an altitude of 3500 m a.s.l. the air temperature shows values down to  
 385  $-27.9^\circ\text{C}$  in winter (Chevuturi et al., 2018) whereas EP had a minimum temperature of just  $-11.6^\circ\text{C}$   
 386 during the study period. Moreover, subzero temperatures were only reached for 7 nights of fountain  
 387 operation at the EP site compared to the 43 nights of fountain operation possible in Ladakh (see Appendix  
 388 8.1). Thus, the Icestupa growth rate is expected to be much higher in Ladakh. However, water spray rates  
 389 in Ladakh are also much higher (around  $210 \text{ l min}^{-1}$ ). This suggests that the water losses in Ladakh could  
 390 be caused by excessive fountain spray.

### 391 6.4 Icestupa construction decisions

392 There are several decisions one has to take when constructing Icestupas. These can be broadly divided  
 393 into two types of decisions, namely location and fountain decisions. Both the meteorological conditions  
 394 of the location and the surface area produced by the fountain significantly influence the observed growth  
 395 rate. Since our validation is restricted to just one location, we restrict our discussion to the optimization  
 396 possibilities of Icestupa constructions through fountain decisions.

397 Assuming a constant spray for the fountain, we can divide the fountain decisions into fountain state  
398 (on/off) and type (height and nozzle diameter). From an energy balance point of view, the fountain should  
399 be switched on for all time intervals when  $q_{net} < 0$ . However, in our experiment, the fountain state  
400 decision was set on the basis of prior Icestupa construction experience where a critical temperature of  
401  $-5^{\circ}C$  was recommended. Ambient temperature can serve as an indicator of  $q_{net}$  as it was correlated  
402 ( $r^2 = 0.53$ ). However,  $q_{net}$  was found to be negative already at a critical temperature of  $-1^{\circ}C$ . Therefore,  
403 using air temperature to determine when the fountain should be switched on is justified but a higher critical  
404 temperature could have been used in the case of the EP Icestupa.

405 The fountain type used can be characterised by the physical structure of the fountain, namely its height and  
406 nozzle diameter. Maintaining the same spray rate and height, one can optimize the Icestupa development  
407 by identifying the minimum nozzle diameter that yields the maximum storage efficiency. Since we never  
408 changed the fountain height for the EP Icestupa, we only focus on optimization of fountain diameter below.

409 Fig. 10 shows reducing the nozzle diameter to  $3\text{ mm}$  increases storage efficiency up to 78 % without  
410 compromising much on storage duration. The corresponding storage quantity of the  $3\text{ mm}$  nozzle diameter  
411 was more than 20 times higher than the  $5\text{ mm}$  fountain used in our experiment. This is because the spray  
412 radius  $r_F$  of the  $3\text{ mm}$  fountain was much higher at  $8.5\text{ m}$  compared to the  $1.7\text{ m}$  spray radius of the  $5$   
413  $\text{mm}$  fountain. Here, we define growth rate as freeze rate when fountain is active and melt rate otherwise.  
414 Therefore, this higher spray radius both increases the freeze rate and increases the melt rate since they are  
415 both directly proportional to the surface area. However, since the freeze rate cannot increase beyond a spray  
416 rate of  $3.6\text{ l min}^{-1}$  (except during precipitation or deposition/condensation events), an optimum spray  
417 radius or nozzle diameter exists, beyond which storage duration suffers due to a disproportionate increase  
418 in melt rate compared to the freeze rate. So even though  $3\text{ mm}$  nozzle diameter had a much higher storage  
419 quantity than the  $5\text{ mm}$  nozzle, its storage duration was around 3 days less than the  $5\text{ mm}$  nozzle. One  
420 physical cause of this effect is the different shapes of both the ice structures. A flat sheet of ice (effectively  
421 a cone with a high spray radius) with higher mass might have a storage duration shorter than a conical ice  
422 structure. As the spray radius decreases with increasing nozzle diameter, the ice structure's average slope  
423 increases and so the  $5\text{ mm}$  nozzle's ice structure is "more" conical than the  $3\text{ mm}$  ice structure. Fig. 10  
424 shows that a nozzle diameter of  $3\text{ mm}$  has an average freeze rate ( $2.4\text{ l min}^{-1}\text{ w.e.}$ ) which is large enough  
425 to increase the storage efficiency and small enough to not reduce the storage duration of the Icestupa  
426 significantly.

## 427 6.5 Artificial snow production vs Artificial ice reservoirs

428 Both artificial snow and ice are produced by expelling small liquid water droplets from the snow gun or  
429 fountain nozzles at high speed (Olefs et al., 2010). The crucial factor that determines ice or snow production  
430 is whether these water droplets remain unfrozen or freeze before reaching the ice/snow surface. According  
431 to (Hartl et al., 2018), the production potential of artificial snowmaking is proportional to the wet-bulb  
432 temperature and the threshold mean daily wet bulb temperature for potential snow making days was  $-2^{\circ}C$   
433 which corresponds well with the threshold mean daily air temperature for potential ice making days of EP  
434 site ( $-1^{\circ}C$ ).

## 7 CONCLUSIONS

435 We outlined a methodology for estimating ice, liquid water, water vapour and runoff quantities produced  
436 during the construction of an Icestupa using measurements of fountain spray rate, air temperature, radiation,  
437 humidity, pressure, wind and cloudiness at the EP study site. The comparison with validation measurements

438 at two different dates during the experiment led to satisfying results, although a more rigorous model  
439 validation was not possible due to few icestupa volume measurements.

440 According to the model, the EP Icestupa achieved a storage quantity of 1005 litres of water with a storage  
441 duration of 65 days. However, the corresponding storage efficiency of 5.4 % was very low for a water  
442 input of 18,560 litres. These estimates were most sensitive to the temperature threshold that determined  
443 precipitation phase and ice emissivity parameters which created an uncertainty of  $0.2m^3$  in the maximum  
444 ice volume calculated. This is to be expected as net longwave radiation and net shortwave radiation together  
445 accounted for around 64 % of the overall energy turnover.

446 Although the location, storage quantity and duration of our experimental EP Icestupa are not representative  
447 of the much larger Icestupas of Ladakh, the model results do support the hypothesis that there could be  
448 considerable water loss during the formation of Icestupas particularly due to excessive fountain spray.  
449 Using model calculations, it was shown that a decreased fountain nozzle diameter of 3 mm can increase the  
450 storage efficiency drastically. This is because a change in the fountain nozzle diameter causes an effective  
451 change of the ice surface area over which the net energy flux can act. This result has relevance on the future  
452 design of Icestupa fountains. However, care has to be taken as our model is currently only validated by one  
453 experiment at the EP site. Further experiments at different locations with different fountains are required to  
454 better understand the influence of construction decisions on the results.

## 8 APPENDIX

### 455 8.1 Ladakh Icestupa 2014/15

456 A 20 m tall Icestupa (Wangchuk, 2015c) was built in Phyang village, Ladakh at an altitude of 3500  
457 m a.s.l. Assuming a conical shape with a diameter of 20 m, the corresponding volume of this Icestupa  
458 becomes  $2093 m^3$  or  $1,920 m^3$  w.e. The fountain sprayed water at a rate of  $210 l min^{-1}$  (Wangchuk,  
459 2015e) from 21<sup>st</sup> January (Wangchuk, 2015a) to at least until 5<sup>th</sup> March 2015 (Wangchuk, 2015b) (around  
460 43 nights). Assuming fountain spray was active for 8 hours each night, we estimate water consumption to  
461 be around  $4,334 m^3$ . Thus, during the construction/freezing period of the Icestupa, roughly 56 % of the  
462 water provided was wasted. The actual water loss is bound to be much higher due to further vapour losses  
463 during the melting period. This Icestupa completely melted away on 6<sup>th</sup> July 2015 (Wangchuk, 2015d).  
464 Therefore, the storage duration was 166 days or roughly 5 months.

## CONFLICT OF INTEREST STATEMENT

465 The authors declare that the research was conducted in the absence of any commercial or financial  
466 relationships that could be construed as a potential conflict of interest.

## AUTHOR CONTRIBUTIONS

467 SB wrote the initial version of the manuscript. MH, ML, SW, JO, and FK commented on the initial  
468 manuscript and helped improve it. SB developed the methodology with inputs from MH. SB performed the  
469 analysis with support from MH and ML. SB and MH participated in the fieldwork.

## FUNDING

470 This work was supported and funded by the University of Fribourg and by the Swiss Government Excellence  
471 Scholarship (Suryanarayanan Balasubramanian).

## ACKNOWLEDGMENTS

472 We thank Mr. Adolf Kaeser and Mr. Flavio Catillaz at Eispalast Schwarzsee for their active participation  
473 in the fieldwork. We would also like to thank Digmesa AG for subsidising their flowmeter used in the  
474 experiment. We would particularly like to thank the editor Prof. Thomas Schuler and 2 anonymous  
475 reviewers who gave us important inputs to improve the paper. We also thank Prof. Christian Hauck, Prof.  
476 Nanna B. Karlsson and Dr. Andrew Tedstone for valuable suggestions that improved the manuscript.

## DATA AVAILABILITY STATEMENT

477 The data and code used to produce results and figures will be published at a later stage and can, until then,  
478 be obtained from the authors upon request.

## REFERENCES

- 479 Apel, H., Abdykerimova, Z., Agalhanova, M., Baimaganbetov, A., Gavrilko, N., Gerlitz, L., et al. (2018).  
480 Statistical forecast of seasonal discharge in central asia using observational records: development of a  
481 generic linear modelling tool for operational water resource management. *Hydrology and Earth System  
482 Sciences* 22, 2225–2254. doi:10.5194/hess-22-2225-2018
- 483 Bonales, L. J., Rodriguez, A. C., and Sanz, P. D. (2017). Thermal conductivity of ice prepared under  
484 different conditions. *International Journal of Food Properties* 20, 610–619. doi:10.1080/10942912.  
485 2017.1306551
- 486 Buck, A. L. (1981). New equations for computing vapor pressure and enhancement factor. *Journal of  
487 Applied Meteorology and Climatology* 20, 1527 – 1532
- 488 Buytaert, W., Moulds, S., Acosta, L., Bievre, B. D., Olmos, C., Villacis, M., et al. (2017). Glacial melt  
489 content of water use in the tropical andes. *Environmental Research Letters* 12, 114014. doi:10.1088/  
490 1748-9326/aa926c
- 491 Chen, Y., Li, W., Deng, H., Fang, G., and Li, Z. (2016). Changes in central asia's water tower: Past, present  
492 and future. *Nature* doi:10.1088/1748-9326/aa926c
- 493 Chevuturi, A., Dimri, A. P., and Thayyen, R. J. (2018). Climate change over leh (ladakh), india. *Theoretical  
494 and Applied Climatology* 131, 531–545. doi:10.1007/s00704-016-1989-1
- 495 [Dataset] Copernicus Climate Change Service (C3S) (2017). Era5: Fifth generation of ecmwf atmospheric  
496 reanalyses of the global climate
- 497 Cuffey, K. M. and Paterson, W. S. B. (2010). *The Physics Of Glaciers* (Elsevier)
- 498 Fujita, K. and Ageta, Y. (2000). Effect of summer accumulation on glacier mass balance on the  
499 tibetan plateau revealed by mass-balance model. *Journal of Glaciology* 46, 244–252. doi:10.3189/  
500 172756500781832945
- 501 Fujita, K., Hiyama, K., Iida, H., and Ageta, Y. (2010). Self-regulated fluctuations in the ablation of a snow  
502 patch over four decades. *Water Resources Research* 46, W11541. doi:10.1029/2009WR008383
- 503 Garratt, J. R. (1992). *The Atmospheric Boundary Layer* (Cambridge University Press)
- 504 Grossman, D. (2015). As himalayan glaciers melt, two towns face the fallout
- 505 Hartl, L., Fischer, A., and Olefs, M. (2018). Analysis of past changes in wet bulb temperature in relation to  
506 snow making conditions based on long term observations austria and germany. *Global and Planetary  
507 Change* 167, 123 – 136
- 508 Hock, R. (2005). Glacier melt: a review of processes and their modelling. *Progress in Physical Geography:  
509 Earth and Environment* 29, 362–391
- 510 Hock, R., Rasul, G., Adler, C., Cáceres, B., Gruber, S., Hirabayashi, Y., et al. (2019). 2019: High mountain  
511 areas. *IPCC Special Report on the Ocean and Cryosphere in a Changing Climate* [H.-O. Pörtner, D.C.

- 512      Roberts, V. Masson-Delmotte, P. Zhai, M. Tignor, E. Poloczanska, K. Mintenbeck, A. Alegria, M. Nicolai,  
513      A. Okem, J. Petzold, B. Rama, N.M. Weyer (eds.)]
- 514      Hoelzle, M., Barandun, M., Bolch, T., Fiddes, J., Gafurov, A., Muccione, V., et al. (2019). *The status and  
515      role of the alpine cryosphere in Central Asia*. doi:10.4324/9780429436475-8
- 516      Hori, M., Aoki, T., Tanikawa, T., Motoyoshi, H., Hachikubo, A., Sugiura, K., et al. (2006). In-situ  
517      measured spectral directional emissivity of snow and ice in the 8–14 micrometer atmospheric window.  
518      *Remote Sensing of Environment* 100, 486 – 502
- 519      [Dataset] IDAWEB (2019). Meteoswiss, federal office of meteorology and climatology
- 520      Immerzeel, W. W., Lutz, A. F., Andrade, M., Bahl, A., Biemans, H., Bolch, T., et al. (2019). Importance  
521      and vulnerability of the world's water towers. *Nature* 577, 364 – 369. doi:10.1038/s41586-019-1822-y
- 522      Meteoblue (2020). Climate schwarzsee
- 523      Mölg, T. and Hardy, D. R. (2004). Ablation and associated energy balance of a horizontal glacier surface  
524      on kilimanjaro. *J. Geophys. Res.-Atmos.* 109, 1–13. doi:10.1029/2003JD004338
- 525      Nüsser, M., Dame, J., Kraus, B., Baghel, R., and Schmidt, S. (2019a). Socio-hydrology of artificial glaciers  
526      in ladakh, india: assessing adaptive strategies in a changing cryosphere. *Regional Environmental Change*  
527      doi:10.1007/s10113-018-1372-0
- 528      Nüsser, M., Dame, J., Parveen, S., Kraus, B., Baghel, R., and Schmidt, S. (2019b). Cryosphere-Fed  
529      Irrigation Networks in the Northwestern Himalaya: Precarious Livelihoods and Adaptation Strategies  
530      Under the Impact of Climate Change. *Mountain Research and Development* 39. doi:10.1659/  
531      MRD-JOURNAL-D-18-00072.1
- 532      Oerlemans, J. and Knap, W. H. (1998). A 1 year record of global radiation and albedo in the  
533      ablation zone of morteratschgletscher, switzerland. *Journal of Glaciology* 44, 231–238. doi:10.  
534      3189/S0022143000002574
- 535      Olefs, M., Fischer, A., and Lang, J. (2010). Boundary conditions for artificial snow production in the  
536      austrian alps. *Journal of Applied Meteorology and Climatology* 49, 1096 – 1113
- 537      Scherrer, S. C. (2020). Temperature monitoring in mountain regions using reanalyses: lessons from the  
538      alps. *Environmental Research Letters* 15, 044005
- 539      Schmidt, L. S., Aðalgeirs ðóttir, G., Guðmundsson, S., Langen, P. L., Pálsson, F., Mottram, R., et al. (2017).  
540      The importance of accurate glacier albedo for estimates of surface mass balance on vatnajökull: evaluating  
541      the surface energy budget in a regional climate model with automatic weather station observations. *The  
542      Cryosphere* 11, 1665–1684. doi:10.5194/tc-11-1665-2017
- 543      Stigter, E. E., Litt, M., Steiner, J. F., Bonekamp, P. N. J., Shea, J. M., Bierkens, M. F. P., et al. (2018).  
544      The importance of snow sublimation on a himalayan glacier. *Frontiers in Earth Science* 6, 108.  
545      doi:10.3389/feart.2018.00108
- 546      Tetens, O. (1930). Über einige meteorologische begriffe. z. *Geophys.* 6, 297–309
- 547      Unger-Shayesteh, K., Vorogushyn, S., Farinotti, D., Gafurov, A., Duethmann, D., Mandychev, A., et al.  
548      (2013). What do we know about past changes in the water cycle of central asian headwaters? a review.  
549      *Global and Planetary Change* 110, 4 – 25. doi:10.1016/j.gloplacha.2013.02.004. Water in Central Asia  
550      – Perspectives under global change
- 551      Wangchuk, S. (2014). Ice stupa artificial glaciers of ladakh
- 552      Wangchuk, S. (2015a). The good news at ice stupa 24th january 2015
- 553      Wangchuk, S. (2015b). Ice stupa artificial glacier inaugurated 5th of march 2015
- 554      Wangchuk, S. (2015c). Ice stupa surpasses guiness world record
- 555      Wangchuk, S. (2015d). Ice stupa way of celebrating a special day
- 556      Wangchuk, S. (2015e). World water day at ice stupa

- 557 WMO (2018). *Guide to Instruments and Methods of Observation* (World Meteorological Organization ;  
558 2018 (2018 Edition))
- 559 Woolf, H. M. (1968). *On the Computation of Solar Elevation Angles and the determination of sunrise and*  
560 *sunset times* (National Aeronautics and Space Administration)
- 561 Zhou, S., Kang, S., Gao, T., and Zhang, G. (2010). Response of zhadang glacier runoff in nam co basin,  
562 tibet, to changes in air temperature and precipitation form. *Chinese Science Bulletin* 55, 2103–2110.  
563 doi:10.1007/s11434-010-3290-5